

Detection of Aerial Spoofing Attacks to LEO Satellite Systems via Deep Learning

Jos Wigchert^a, Savio Sciancalepore^{a,*}, Gabriele Oligeri^b

^aEindhoven University of Technology (TU/e), Eindhoven, Netherlands

^bHamad Bin Khalifa University (HBKU), College of Science and Engineering (CSE), Doha, Qatar

Abstract

Detecting spoofing attacks to Low-Earth-Orbit (LEO) satellite systems is a cornerstone to assessing the authenticity of the received information and guaranteeing robust service delivery in several application domains. The solutions available today for spoofing detection either rely on additional communication systems, receivers, and antennas, or require mobile deployments. Detection systems working at the Physical (PHY) layer of the satellite communication link also require time-consuming and energy-hungry training processes on all satellites of the constellation, and rely on the availability of spoofed data, which are often challenging to collect. Moreover, none of such contributions investigate the feasibility of aerial spoofing attacks launched via drones operating at various altitudes. In this paper, we first show experimentally the viability and effectiveness of spoofing attacks to LEO satellite systems using aerial attackers deployed on drones. We also propose a new spoofing detection technique, relying on pre-processing raw physical-layer signals into images and then applying anomaly detection on such images via autoencoders. We validate our solution through an extensive measurement campaign involving the deployment of an actual spoofer (Software-Defined Radio) installed on a drone and injecting rogue IRIDIUM messages while flying at different altitudes with various movement patterns. Our results demonstrate that the proposed technique can reliably detect LEO spoofing attacks launched at different altitudes, while state-of-the-art competing approaches simply fail. We also release the collected data as open source, fostering further research on satellite security.

Keywords: Wireless Security, Satellite Security, Artificial Intelligence for Security, Mobile Security, Drones

1. Introduction

Low-Earth Orbit (LEO) satellite communication systems have recently gained renewed momentum in Internet of Things (IoT) research and Industry, thanks to the enhanced efficiency, simplicity, and low cost in technology access [1] [2]. Several commercial IoT-based applications are also benefiting from the integration of such a technology, with new powerful satellite-based services emerging like real-time data collection, predictive maintenance, asset tracking, cold-chain management, and resource exploration, to name a few, and new communication paradigms appearing, e.g., Mobile Edge Computing [3].

At the same time, the existence of a satellite communication link also increases the threat surface of such users. Among the various cybersecurity threats affecting LEO satellite systems, *spoofing attacks*, a.k.a. *wireless impersonation*, exploit the absence (or compromise) of message authentication techniques to

inject rogue messages on the satellite link [4]. Such messages are crafted to be indistinguishable from legitimate ones, being received and processed by commercial satellite receivers, leading to successful attacks [5], [6].

Many solutions are available in the literature for the detection of satellite spoofing [7], [8]. However, they require several communication systems, receivers and antennas, or mobile systems distributed in a large area, being quite expensive to deploy for many application domains. When considering standalone non-mobile systems, the literature suggests the use of transmitter identification approaches, as in [9], or the usage of fading phenomena to detect spoofing, as in [10] and [11]. However, these solutions require binary classification, building on top of time- and resource-consuming training processes involving both legitimate and spoofed signals, which are often either impractical or unlawful to acquire. Some scientific contributions such as [7] and [5] identified the feasibility of spoofing attacks to LEO satellite systems, while some others identified the threats posed by aerial spoofing platforms, such as Kumar et al. [12]. However, none of the contributions available in the literature for satellite spoofing detection provide solutions that do not require the availability of attack data during system training. Also, none of these works perform real-world experimentation with aerial spoofing attacks carried out by drones hovering or flying at various altitudes. Using such a strategy, the adversary could mimic better the satellite downlink to avoid detection and maximize damage.

*This work has been partially supported by the INTERSECT project, Grant No. NWA.1162.18.301, funded by the Netherlands Organization for Scientific Research (NWO). Any opinions, findings, conclusions, or recommendations expressed in this work are those of the author(s) and do not necessarily reflect the views of NWO. Moreover, this publication was made possible by the NPRP12C-0814-190012-SP165 awards from the Qatar National Research Fund (a member of Qatar Foundation).

*Corresponding author

Email addresses: j.wigchert@student.tue.nl (Jos Wigchert), s.sciancalepore@tue.nl (Savio Sciancalepore), goligeri@hbku.edu.qa (Gabriele Oligeri)

Contribution. In this paper, we provide the following contributions: (i) we demonstrate the technical feasibility of *aerial spoofing* attacks to LEO satellite systems, where an adversary uses drones operating at various altitudes (beyond Line-of-Sight) to stealthily inject spoofed messages to a target satellite receiver; (ii) we demonstrate that existing solutions to detect LEO spoofing attacks fail to discover such attacks, misclassifying spoofed messages as legitimate ones; (iii) we design a new solution for aerial spoofing attacks to LEO satellite systems, pre-processing raw IQ samples into images and using a sparse Autoencoder (AE) to reliably detect anomalies in the received signals; and finally, (iv) through extensive real-world experimentation involving actual drones and Software-Defined Radios (SDRs), we demonstrate the robustness and effectiveness of our proposed solution and its superior performances against the state of the art. To the best of our knowledge, this paper is the first to consider real-world aerial spoofing attacks to LEO satellite systems and to propose an ad-hoc pre-processing technique of physical-layer information enabling attack detection via sparse AE. Although similar techniques have been applied for identifying specific satellites, e.g., in [9], we demonstrate experimentally that satellite link fingerprinting is better suited for detecting spoofing attacks compared to identifying single satellites. We also release the dataset collected for this work at [13], enabling further research on LEO satellite links modeling, monitoring, and security.

We highlight that this paper extends our previous research in [10] and [11] through the following new contributions:

- We demonstrate the technical feasibility of aerial spoofing attacks to LEO satellite systems, using a drone operating at various altitudes to inject replayed IRIDIUM messages to a receiver on the ground.
- While previous research leveraged binary classification for spoofing detection, in this paper, we demonstrate the feasibility of detecting spoofing attacks to LEO satellite systems using a pre-processing technique transforming physical-layer information into images, enabling spoofing detection through one-class classification via autoencoders, thus requiring the availability of only regular communication samples at training time.
- While previous research demonstrated the effectiveness of fading fingerprinting by only considering terrestrial attacks, in this paper, we consider a novel attack strategy, i.e., aerial spoofing attacks launched through drones.
- We collect a brand new real-world dataset, including benign satellite data and actual spoofing attacks carried out using SDRs and drones, and release this dataset as open source to the research community at [13].
- We compare the performance of our newly proposed approach against preliminary solutions proposed in [11] and [9], demonstrating the superiority of our approach in terms of attack detection accuracy while also requiring fewer samples than competing solutions.

Roadmap. This paper is organized as follows. Sec. 2 introduces the preliminaries, Sec. 3 reviews related work, Sec. 4 introduces the system and adversary model, Sec. 5 provides the details of our solution, Sec. 6 describes our data collection, Sec. 7 provides the results, Sec. 8 discusses implications and limitations of our research, and finally, Sec. 9 draws the conclusion.

2. Background

This section introduces preliminary concepts, i.e., digital modulation principles, used as an input to detecting spoofing attacks, the IRIDIUM satellite infrastructure, used for our experimental testing phase, and AEs, used as part of our detection solution.

Digital (De-)Modulation. Modern wireless communication technologies use digital modulation to make bit-strings suitable for transmission over the Radio Frequency (RF) link. Such signals are typically expressed in the form of a complex number $I + jQ$, namely In-Phase Quadrature (IQ) samples, being I the *In-Phase* and Q the *Quadrature* component. These components are (90 degrees) phase-shifted by the transmitter before transmission so that they do not interfere with each other while propagating over the wireless channel. The original IQ value (and bitstream) can be recovered by the receiver by multiplying the received signal via two orthogonal tones [14]. The number of possible symbols s defined by the modulation scheme, i.e., $\log_2 s$ bits/sec, impacts the throughput of the communication link. In addition, s defines the tolerance of the communication link to noise. In fact, the IQ symbols at the receiver are affected by noise n , introduced jointly by the electronics of the transmitter and the communication channel. The receiver simply maps the received IQ symbol $x = I + jQ + n$ to the closer expected one, i.e., the symbol characterized by the minimum error. The higher the noise power, the higher the probability that a symbol is distorted enough to get closer to another one, causing a decoding error. Thus, communication links affected by high noise, such as satellite links, use lower-order schemes, e.g., Binary Phase Shift Keying (BPSK) ($s = 2$) and Quadrature Phase Shift Keying (QPSK) ($s = 4$), trading off throughput with robustness to noise. Also, note that Commercial-Off-The-Shelves (COTSs) cannot easily control the value of the IQ samples. Indeed, the IQ samples received by a device are affected by both manufacturing inaccuracies in the transmitter hardware, which are inherent to such devices, and fading phenomena caused by the wireless channel [15]. In our paper, we analyze the distortion affecting the IQ samples received by a target user to detect spoofing attacks (see Sec. 5).

IRIDIUM. IRIDIUM is a LEO satellite constellation operated by IRIDIUM Communications Inc, offering global satellite phone and data coverage currently to more than 2 millions users [16], [17]. IRIDIUM enables users to communicate from anywhere on Earth, including remote areas where traditional terrestrial communication networks typically cannot provide connectivity. The constellation includes 66 LEO satellites orbiting at 800 km all over the Earth's surface and moving from north to

south [18]. The satellites transmit messages in the frequency band $[1,618.75 - 1,626.5]$ MHz using the modulation scheme Differential QPSK (DQPSK), which can be received through dedicated satellite receiving stations provided by authorized resellers such as Motorola and Kyocera. IRIDIUM features two main types of communication channels, i.e., *system overhead* and *bearer service* channels [19]. Some channels are authenticated, while others are not authenticated and not encrypted, allowing for spoofing attacks. Unauthenticated and unencrypted channels, e.g., IRIDIUM Ring Alert (IRA), are used to broadcast information about a specific satellite. The information delivered by satellites on such channels can be detected and decoded using a SDR, a generic active antenna, and a software development kit like *gr-iridium* [20]. IRIDIUM satellites serve primarily as a communication system. However, the network can also be used for positioning purposes, e.g., through systems like *DDK Positioning* [21]. IRIDIUM also features a dedicated IRIDIUM IoT service, specifically dedicated to Machine-to-Machine (M2M) applications like transportation, agriculture, oil and gas, utilities, and construction, among many others [22]. In this paper, we use IRIDIUM as the reference LEO satellite constellation to test spoofing attacks because of its popularity, number of users, and availability of an open-source reception module for SDRs to receive real messages, enabling our experimental data collection and analysis.

Autoencoders (AE). AEs are special types of neural network architectures used for unsupervised learning tasks, including anomaly detection and dimensionality reduction [23]. They feature an encoder, compressing the input data M into a lower-dimensional representation, and a decoder, that reconstructs the original data from such compressed representation. The encoder function G_θ maps the input image M to a latent representation $z \in \mathbb{R}^d$, through a transformation of the type $z = G_\theta(M)$, where θ represents the encoder function with related parameters and d is the dimensionality of the latent space, typically much smaller than the original image dimensions $M_W \times M_H$ [24]. The decoder function F_ϕ maps the latent representation back to the reconstructed image \hat{M} , through the transformation $\hat{M} = F_\phi(z)$, being (ϕ) the decoder transfer function with specific decoder parameters. AEs are trained to minimize the reconstruction error \mathcal{L} between the original input image M and the reconstructed image \hat{M} , measured using the Mean Squared Error (MSE) loss function, as in Eq. 1 [25].

$$\mathcal{L}(\theta, \phi) = \frac{1}{M_W M_H} \sum_{i=1}^{M_W} \sum_{j=1}^{M_H} (M_{i,j} - \hat{M}_{i,j})^2. \quad (1)$$

Note that AEs can also be used as a one-class classification tool, i.e., they can be trained only on samples from one class and then used to detect anomalies as outliers. This is particularly useful when dealing with aerial spoofing attacks. Indeed, collecting attack samples (anomalies) is particularly challenging because of the equipment, technical difficulties required to assemble the experimental setup and launch the attack, and finally, law and safety regulations, which often prevent the collection of such data. Recent related work, such as the one by the

authors in [26], also identified experimentally the advantage of autoencoder-based models when a limited number of anomalous samples is available. We use this feature as part of our solution (see Sec. 5).

3. Related Work

Spoofing of satellite messages is usually associated with Global Navigation Satellite System (GNSS) spoofing, i.e., the falsification of positioning and navigation messages emitted by systems such as GPS, GALILEO, and GLONASS [36]. Although secure versions of such communication technologies exist and are used by the military, for backwards-compatibility reasons, civilian systems mostly use their former versions, which are insecure by design. In this context, He et al. in [37] also identified that, similarly to GNSS technologies like GPS, LEO satellite networks typically use a dedicated downlink pilot channel for broadcasting channel status, user management information, call information, etc., as exemplified by Iridium. Attackers can imitate the dedicated pilot channel to broadcast false information to legitimate users, causing network paralysis. However, they did not provide valid countermeasures for such attacks. One common strategy to detect spoofing attacks involves the exploration of alternative sources, such as military GNSS signals [31], terrestrial communication systems [38], or the integration of data from additional GNSS constellations, such as Iridium [18]. These methodologies utilize the correlation between the information collected in distinct channels to assess the authenticity of GNSS signals. However, they depend on the availability and authenticity of an alternative source of information. Some other proposals, such as [30], use multiple receivers to detect spoofing attacks, leveraging spatial and channel diversity and the use of Channel State Information (CSI)-based fingerprints of the received signal. This approach has also been used by the authors in [27] and [32] for WiFi signals, and is overall very promising for indoor spoofing detection. However, as shown in Sec. 7.2, it hardly applies to GNSS spoofing due to high channel noise. To create channel diversity without several receivers, the authors in [33] use a mobile Global Positioning System (GPS) receiver. However, such solutions require mobile receivers and usually incur a non-negligible delay, necessary to actually move from one location to another. Recent popular methods to detect (GNSS) spoofing attacks involve the use of Radio Frequency Fingerprinting (RFF), i.e., the creation of a transmitter fingerprint that helps distinguish legitimate from rogue ones. RFF has been applied successfully for terrestrial communication technologies [39], LEO [9], [40], [41], and GPS satellites [28]. However, it requires significant training time and does not scale up with the number of legitimate satellites, which is typically large for LEO constellations. Other proposals in the GNSS domain, such as the one by Borhani et al. in [42], use GNSS-specific metrics, such as Cross Ambiguity Function (CAF), to detect spoofing attacks. Being such metrics specific to GNSS technologies, they cannot be used for LEO satellite spoofing detection. Some more recent proposals, such as [10], [11], and [29], use IQ samples to detect spoofing attacks affecting both the LEO and GNSS constellations. While

Paper	Location Independence	Single Receiver	Support for Static Receivers	No crypto	No Multiple Sources	Applied on Satellites	No Binary Classification	Aerial Adversary
[11]	●	●	●	●	●	●	○	○
[12]	●	●	●	●	●	●	○	○
[27]	○	●	●	●	●	○	○	○
[18]	●	●	●	●	○	●	○	○
[28]	●	●	●	●	●	●	○	○
[29]	○	●	●	●	●	●	●	○
[30]	○	○	●	○	●	○	○	○
[31]	●	○	●	●	○	●	●	○
[32]	●	●	●	●	●	○	○	○
[33]	●	●	○	○	●	●	●	○
[34]	○	●	●	●	●	●	●	○
[35]	○	●	●	●	●	●	●	○
Ours	●	●	●	●	●	●	●	●

Table 1: Related work on Spoofing Detection.

the authors in [29] detect anomalies in the Quadrature component of IQ signals, the proposals in [10] and [11] apply binary classification to both I and Q components to detect spoofing and require knowledge of both spoofed and legitimate samples. Binary classification is also required by Kumar et al. in [12], which applied Long Short-Term Memory (LSTM) to noise data via simulations to detect aerial spoofing. It is also worth mentioning the contributions by Abdrabou et al. in [34] and [35], using Doppler frequency shift (DS) and received power (RP) features to detect spoofing attacks to satellite systems. However, none of these solutions take into account spoofing attacks carried out by aerial attackers, such as drones.

Thus, as summarized in Table 1, the current literature misses actual real-world tests involving spoofing attacks from aerial adversaries. Moreover, existing methods cannot provide a scalable mechanism independent of the number of satellites that comprise the LEO constellation. In Sec. 7.2, we also compare our solution to the solutions proposed in [11] and [9], demonstrating superior performance.

4. System and Adversary Model

Figure 1 illustrates the system and adversary models considered in this work.

Our reference scenario includes three relevant entities: (i) the satellite transmitter, (ii) the user equipped with a satellite receiver, and (iii) the adversary.

Without loss of generality, we consider a satellite transmitter located in the LEO, emitting RF messages according to the IRIIDIUM communication system, as discussed in Sec. 2. Thus, legitimate signals emitted by the satellite follow the modulation scheme QPSK with differential encoding, a.k.a. DQPSK, and are transmitted in the frequency band [1, 618.725–1, 626.5] MHz. The user features a receiving device able to receive and decode IRIIDIUM satellite messages, e.g., for communication in hard-to-reach locations. We consider a receiver deployed outdoors for maximum satellite visibility. We do not make any additional assumptions on the deployment of the receiver, which

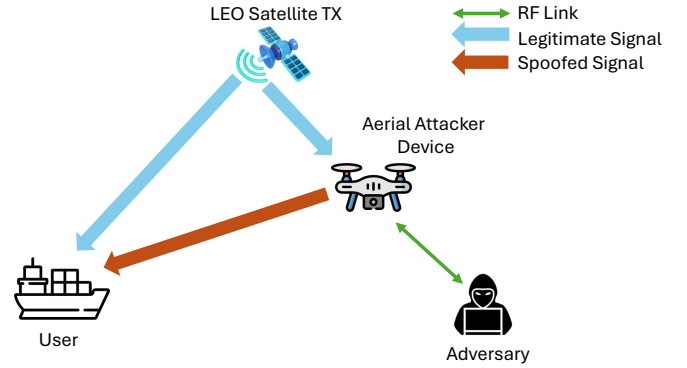


Figure 1: System and adversary model. An adversary deploys a drone to spoof LEO satellite messages delivered by legitimate satellites at a target receiver.

can be either static or mobile. However, we consider that the user does not feature any additional Internet connection than the one possibly provided by the LEO satellite system. Thus, the user cannot resort to any other service than the IRIIDIUM communication system to verify the legitimacy of the information provided through such a system. This consideration applies to many IRIIDIUM deployments, as the system is typically used to enable communications in remote and hard-to-reach locations. Moreover, note that we require raw physical-layer IQ data to detect spoofing attacks. Such data are usually not available when using COTSs, while they are available by using SDRs, as we did in our experimental campaign. Thus, users willing to deploy our solution require a SDR to collect the data aside to the IRIIDIUM receiver provided by the service provider.

Adversary Model. The adversary considered in this work, namely \mathcal{A} , aims to spoof satellite messages, making them appear legitimate to the user for processing. The adversary’s objective is to induce the computation of a different position, velocity, and/or time (PVT) in a targeted civilian IRIIDIUM receiver. This objective is feasible since many (LEO) satellite systems, including IRIIDIUM, use unencrypted and unauthenticated messages. In addition, messages transmitted from LEO

satellites typically arrive at the receiver with low Signal-to-Noise Ratio (SNR), and they are easily overcome in terms of power by the ones injected by the adversary. In practice, \mathcal{A} can use a SDR to both eavesdrop on legitimate messages delivered by legitimate IRIDIUM satellites, and inject new spoofed messages on the communication channel. In this paper, we specifically consider the scenario in which \mathcal{A} uses an Unmanned Aerial Vehicle (UAV), a.k.a. drone, to launch replay (meaconing) and spoofing attacks. The use of a drone as a transmitting source makes the received signal (and the associated fading phenomenon) more similar to a satellite downlink, thus having higher chances to bypass (state-of-the-art) spoofing detection solutions based on fading fingerprinting, such as the ones in [10] and [11]. The objective of this paper is to discriminate legitimate (benign) from spoofed (malicious) IRIDIUM messages through the analysis of the information available at the physical layer of the communication link.

5. Satellite Spoofing Detection

In this section, we describe the methodology used to detect spoofing attacks to LEO satellite communication systems. Our proposed methodology for spoofing detection is divided into two phases, i.e., *image generation* from physical layer information, i.e., IQ samples, (see Sec. 5.1) and *spoofing detection* (Sec. 5.2). Tab. 2 summarizes our main notation.

Symbol	Description
I_k	In-phase component of the k -th IQ sample.
Q_k	Quadrature component of the k -th IQ sample.
N	Total number of IQ samples.
P	Number of histogram bins along the I axis.
Q	Number of histogram bins along the Q axis.
$b_{I,j}$	j -th bin edge along the I axis.
$b_{Q,j}$	j -th bin edge along the Q axis.
$H_{i,j}$	Value of the histogram at bin (i, j) .
$M_{i,j}$	Value of the image at pixel (i, j) .
$\mathbb{I}(\circ)$	Indicator function.
L	Number of neurons of the encoder of the AE.
S	Number of neurons of the decoder of the AE.
$\mathbf{MSE}_{\text{train}}$	Vector of MSE values generated during AE training.
τ	Threshold of the AE.
$E(\circ)$	Mean operator.
$\sigma(\circ)$	Standard Deviation operator.

Table 2: Notation and description.

5.1. Image Generation

Figure 2 shows the image generation methodology used in our approach. Our solution analyzes raw IQ samples, collected through a device capable of extracting Physical (PHY)-layer data from the received signal, e.g., a SDR or a spectrum analyzer. We divide the stream of IQ samples into subsets (non-overlapping chunks) of N samples, i.e., $\{(I_k, Q_k)\}_{k=1}^N$ (see Sec. 7.2 for an evaluation of the impact of N on the performance of our solution), and visualize them through an IQ constellation diagram, with the I component on the x-axis and the Q component

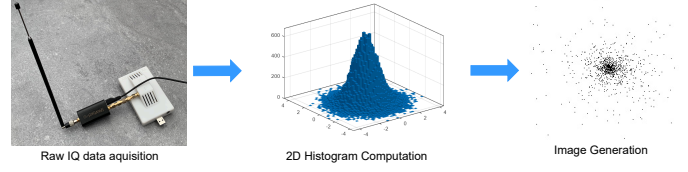


Figure 2: Graphical overview of the image generation methodology used in our solution.

on the y-axis. Then we divide the diagram into a $P \times Q$ grid, with P and Q chosen according to the methodology used for spoofing detection (see Sec. 5.2). We count how many samples fall into each tile of the grid, so generating a histogram H . Denoting with \mathbf{b}_I and \mathbf{b}_Q the set of edges of the tiles of the histogram along X and Y , respectively, the value of the histogram tile $H_{i,j}$ follows Eq. 2.

$$H_{i,j} = \sum_{k=1}^N \mathbb{I}(b_{I,i} \leq I_k < b_{I,i+1}) \cdot \mathbb{I}(b_{Q,j} \leq Q_k < b_{Q,j+1}), \quad (2)$$

where \mathbb{I} is the indicator function, defined as per Eq. 3.

$$\mathbb{I}(\circ) = \begin{cases} 1 & \text{if } \circ \text{ evaluates to true,} \\ 0 & \text{otherwise.} \end{cases} \quad (3)$$

We interpret each tile of the histogram as a pixel of a grey-scale image, where 0 is black and 255 is white. If $N > 255$, it is possible that $H_{i,j} > 255$; in such a case, we truncate such a value to 255. Finally, we provide the resulting matrix (image) as input for the following spoofing detection phase. Note that, by converting IQ samples into an image, we provide the AE with a structured representation of the RF signal, facilitating effective learning and anomaly detection.

5.2. Spoofing Detection via Autoencoders

We identify a spoofing attack using sparse AEs, by detecting anomalies in the images generated from the received RF signal due to different fading phenomena affecting the communication link (satellite vs aerial). In particular, the shape of the IQ clouds at the receiver when considering benign and malicious signals is different—the signal received from the spoofer installed on the drone has more statistical variance around the expected values than the signal received from the satellites. We attribute this phenomenon to the different fading phenomena affecting the received signals, as the signal generated by the satellites comes from a different altitude than the one originated by the spoofer on the drone, being subject to different fading.

According to such considerations, the key design objective of our solution is to learn an efficient, compressed representation (encoding) of the input IQ data, for the purpose of feature learning, while being able to reconstruct the original input as accurately as possible from this encoding. Using mathematical notation, considering: (i) the input \mathbf{x} (image generated from N IQ samples), (ii) the encoder function f_θ , with θ being a parameter that maps \mathbf{x} over the latent representation \mathbf{z} , (iii) the decoder function $g(\phi)$, being ϕ a parameter that is used for decoding \mathbf{z}

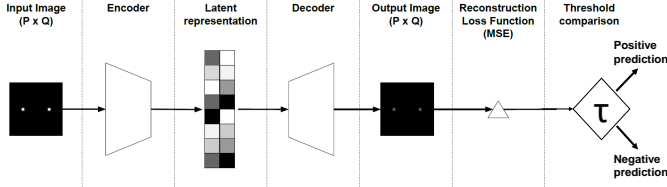


Figure 3: AE-based spoofing detection architecture.

into a reconstruction of the input $\tilde{\mathbf{x}}$, and (iv) $\hat{\mathbf{x}} = g_\phi(f_\theta(\mathbf{x}))$ the reconstruction of the input, the objective of our autoencoder is to minimize the reconstruction loss as defined in [43] over the dataset of the training images D , according to Eq. 4:

$$\min_{\theta, \phi} \mathbb{E}_{\mathbf{x} \sim D} [\mathcal{L}(\mathbf{x}, \hat{\mathbf{x}})] = \min_{\theta, \phi} \mathbb{E}_{\mathbf{x} \sim D} [\mathcal{L}(\mathbf{x}, g_\phi(f_\theta(\mathbf{x})))] \|\cdot\|_2^2, \quad (4)$$

where \mathcal{L} is the reconstruction loss function introduced in Eq. 1.

Figure 3 shows the architecture of the adopted AE. We provide images (generated through the procedure described in Sec. 5.1) as input to an encoder using a logarithmic sigmoid activation function with $L = 16$ neurons. Such an operation generates a compressed latent representation of the input image, characterized by $L = 16$ dimensions. Specifically, our encoder generates the latent representation \mathbf{z} according to Eq. 5:

$$\mathbf{z} = \sigma(W^{(1)}\mathbf{x} + \mathbf{b}^{(1)}), \quad (5)$$

where $(W^{(1)} \in \mathbb{R}^{16 \times n})$ is the encoder weight matrix, $(\mathbf{b}^{(1)} \in \mathbb{R}^{16})$ is the bias vector of the encoder and $\sigma(s) = \frac{1}{1+e^{-s}}$ is the sigmoid activation function. We feed such a latent representation vector \mathbf{z} to a decoder using a linear decoder transfer function, using $S = 50,176$ neurons. Our AE architecture uses two hidden layers, the optimizer algorithm Limited-memory Broyden–Fletcher–Goldfarb–Shanno (L-BFGS) algorithm, and the sparsity regularization technique. Thus, the operations performed by the decoder to obtain the reconstructed input $\hat{\mathbf{x}}$ can be expressed as in Eq. 6.

$$\begin{aligned} \mathbf{z}^{(2)} &= \phi^{(2)}(W^{(2)}\mathbf{z}^{(1)} + \mathbf{b}^{(2)}), & \mathbf{z}^{(2)} &\in \mathbb{R}^{h_2} \\ \mathbf{z}^{(3)} &= \phi^{(3)}(W^{(3)}\mathbf{z}^{(2)} + \mathbf{b}^{(3)}), & \mathbf{z}^{(3)} &\in \mathbb{R}^{h_3} \\ \hat{\mathbf{x}} &= W^{(4)}\mathbf{z}^{(3)} + \mathbf{b}^{(4)}, & \hat{\mathbf{x}} &\in \mathbb{R}^{50176} \end{aligned} \quad (6)$$

where $(\phi^{(2)}, \phi^{(3)})$ are activation functions for decoder hidden layers, $(W^{(2)}, W^{(3)}, W^{(4)})$ are weights for each decoder layer, $(\mathbf{b}^{(2)}, \mathbf{b}^{(3)})$, are biases for each decoder layer, and $\mathbf{z}^{(2)}$ and $\mathbf{z}^{(3)}$ represent the intermediate activations (or outputs) of each decoder hidden layer, namely the hidden states. Note that, in line with general principles of autoencoders (see [43]), for a deep network with L layers there are $L + 1$ weight matrices, i.e., one for each layer and one final weight matrix to project from the last hidden layer to the output. We obtain as output $\hat{\mathbf{x}}$ an image of the same size as the input $(P \times Q)$, which we convert into a matrix and compare with the input image through the MSE loss function, as in Eq. 1 (Sec. 2).

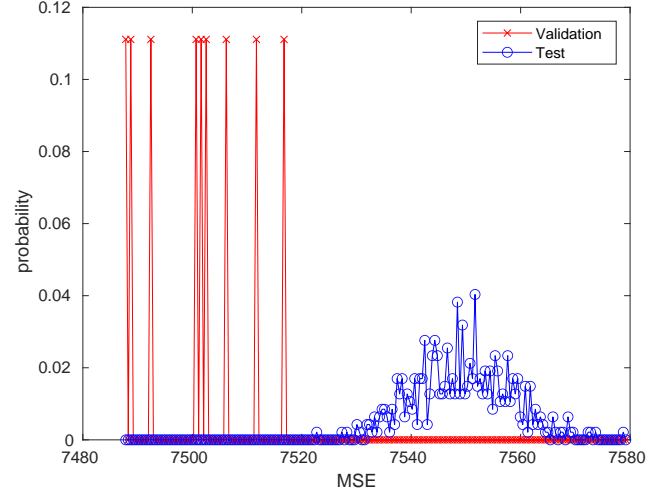


Figure 4: Distribution of MSE values from our dataset: red crosses represent MSE computed on satellite images, and blue circles represent MSE values computed on images generated from the aerial link (drone).

Our approach involves *training* and *testing*. For the training process, we use only images generated from IQ samples captured from legitimate LEO satellite communications, generating a set of MSE values characterizing the regular pattern of the communication link, namely $\mathbf{MSE}_{\text{train}}$. We use such values to compute the threshold τ , used to differentiate images generated from legitimate satellites from spoofed ones. An image with $MSE \leq \tau$ is predicted to be generated from legitimate transmitters (LEO satellites), while an image with $MSE > \tau$ is predicted to be generated from unauthorized entities (adversary). For computing τ , we use Eq. 7, as proposed by the authors in [44] (Sec.4.1), so as to take into account as much as possible the variability of legitimate communication patterns due to noise.

$$\tau = E(\mathbf{MSE}_{\text{train}}) + 3 \cdot \sigma(\mathbf{MSE}_{\text{train}}), \quad (7)$$

where $E(\circ)$ and $\sigma(\circ)$ represent the mean and the standard deviation, respectively.

An image generated from satellite samples is characterized by lower MSE values. In contrast, an image generated from a transmitter at a lower altitude (terrestrial or aerial) results in a higher MSE value. We show a sample distribution of the MSEs in Fig. 4. Note that images generated from satellite data are characterized by a higher probability of having lower MSE values compared to images generated from data spoofed by the drone. Thus, by considering a discrimination threshold, we can detect spoofing attacks as anomalies in the resulting MSE values. Note that we empirically select a hidden size value of 16, a sparsity regularization term of 0.5, an L2-regularization term of 0.01, and 250 epochs for the training. Such values were selected through experimental fine-tuning based on the available data (see later section).

6. Data Collection

In this section, we describe the experimental setup used for data collection (Sec. 6.1), the experiment settings (Sec. 6.2),

and we report on a preliminary statistical analysis of our measurements (Sec. 6.3).

6.1. Experimental Setup

Hardware Details. To collect the data required to test our solution, we use two SDRs *LimeSDR USB*. This hardware has a frequency range of 100 kHz up to 3.8 GHz, a maximum bandwidth of 61.44 MHz, and a transmit power of up to 10 dBm. One LimeSDR is used as a receiver of the IQ samples (the user in our scenario). To boost message reception, we use the Low-Noise Amplifier (LNA) module *Nooelec SAWbird+IR*, characterized by high attenuation outside of the 60MHz bandpass region centered around 1.620GHz, and a minimum of 20dB of gain within the bandpass region, being suitable for receiving messages in the bandwidth of our interest [45]. We connect the receiving LimeSDR and the LNA to a telescopic antenna, extendable on purpose to maximize access to the open sky. Finally, we connect the LimeSDR USB to a laptop, running software used to communicate with the SDR. Figure 5(a) illustrates the overall receiver (RX) setup. Another LimeSDR is used as a transmitter (spoofer) of IRIDIUM messages and installed on-board a drone. We use the drone DJI Phantom 1, characterized by a maximum vertical speed of 6 m/s, maximum horizontal speed of 10 m/s, and a flight time of approx. 15 minutes. On-board the drone, besides the LimeSDR (weighting 49 g), we install the embedded computer Raspberry Pi 4, allowing us to control the LimeSDR and weighting 87 g, and a power bank *TNTOR 3500mAh*, weighting 94 g and providing enough input power to the Raspberry Pi (see Fig. 5(b)). To hold all such components together in a safe way, we use 3D-printed parts weighing approx. 20 g, for a total payload weight of 250 g that can be carried by the selected drone with no impact on stability and maneuverability [46], [47]. With such a weight onboard, the drone battery lasts approx. 10 minutes at 120 m, allowing us to gather enough data for our experiments. We show the overall transmitter setup in Fig. 5(c).

Software Details. On the laptop connected to the receiver, we use the state-of-the-art software *iridium-extractor* for receiving and decoding IRIDIUM messages [20]. We modified the tool to output raw IQ samples of decoded packets besides the demodulated bits of the messages. To transmit valid IRIDIUM messages, we first collected locally a dataset of legitimate IRIDIUM packets, and then used the LimeSDR installed on the drone to replay such packets on the same carrier frequency used by legitimate IRIDIUM communications, through the same modulation (DQPSK). To do this, we created a custom flow chart using GNURadio, a popular software development toolkit for SDRs, and we verified that our injected IRIDIUM messages are received and processed with no errors by *gr-iridium*, as legitimate messages. To enable message injection on the LimeSDR installed on the drone, we connect via SSH to the Raspberry Pi on a wireless connection through our laptop, and we use a Tmux session to allow our program to run also when the SSH session is closed.

6.2. Experiment Settings

We deployed the described experimental setup at a rural field located about 1.5 km northeast of Herwijnen, in the Netherlands, shown in Fig. 6. The field is located at a minimum distance of approx. 500 m from any man-made construction, offering an ideal place to fly the drone while minimizing safety concerns. Moreover, for reproducibility purposes, note that there is only grass at the ground level that impacts the profile of the signal received from satellites and drones. At this location, we acquired legitimate and spoofed data while considering the following three scenarios:

- *S1: Outdoor - Static.* We consider the receiver stationary on the ground and the transmitter drone hovering in the air, at increasing altitude up to 120 m, i.e., the maximum allowed altitude for a drone in our area [48].
- *S2: Outdoor - Moving Transmitter.* We consider the receiver stationary on the ground and the transmitter on the drone moving in the air at increasing altitude up to 120 m, in a circle of radius ≈ 15 m around the receiver. We flew this movement manually by moving the sticks on the remote controller. This scenario aims to estimate the detection performance when the adversary implements evasion techniques by moving itself (flying around).
- *S3: Outdoor - Moving Receiver and Transmitter.* We consider both the receiver and the transmitter moving in a circle of radius ≈ 15 m from the starting location, coincidental with the receiver location in S1 and S2. We let the drone fly at an increasing altitude, up to 120 m. During the experiments, the transmitter and receiver experience various (random) distances. This scenario aims to investigate the impact of receiver movement on the capability to detect spoofing.

We believe that such scenarios cover the most realistic cases of aerial spoofing attacks to LEO satellite receivers deployed outdoors, making our results generalizable to any receivers deployed outdoors in a scenario like the one shown in Fig. 6. Moreover, our experiments consider various movement patterns, accounting for heterogeneous noise patterns, multipath, and interference conditions characterizing real-world satellite communication channels. Our experiments also cover multiple altitudes and fading dynamics, addressing possible concerns about the limited scalability and robustness of our experimental findings. Note that, to avoid interfering with other potential IRIDIUM receivers in the area, we selected a TX power gain value on the transmitter low enough not to generate interference further away than 500 m, while being high enough to still receive messages from the maximum altitude of 120 m. Finally, note that we did not perform new measurements for ground-based spoofing attacks, as such scenarios are already covered by the literature [11].

6.3. Data Analysis

Our collected dataset includes more than 10,000 legitimate IRIDIUM messages. Moreover, we collected more than 1,000



(a) Receiver setup.



(b) Spoofing setup



(c) Spoofing setup mounted on the drone.

Figure 5: Experimental setup, including the receiver setup (a), spoofing setup (b) and spoofer installation on the drone (c).



Figure 6: Photo of the data collection site.

spoofed IRIDIUM messages for each scenario and tested altitude, as summarized in Tab. 3, for a total number of approx. 24,000 messages. Our dataset is available as open source at [13]. First, note that our IRIDIUM receiver detects all the spoofed

Experiment	Altitude [m]	Messages [#]
S1	10	1110
	30	1008
	50	1163
	70	1133
	90	1263
	120	1104
S2	30	1189
	70	1178
	120	1238
S3	30	1169
	70	1085
	120	1239

Table 3: Collected spoofed messages.

messages as legitimate IRIDIUM messages, as they were delivered from IRIDIUM satellites. This successful experiment demonstrates the feasibility of launching (aerial) spoofing attacks to a LEO satellite constellation, i.e., IRIDIUM, using the unencrypted broadcast channel IRIDIUM Ring Alert. We report in Fig. 7 example images generated from $N = 1,000$ le-

gitimate and spoofed IQ samples, highlighting the similarity of the received data when the user is subject to spoofing attacks compared to a benign scenario. When comparing the images in Fig. 7 with the images in Fig. 8, reporting the profile of the received IQ samples collected from ground-based spoofers as part of the analysis carried out in the preliminary contribution in [11], it is immediate to visualize that aerial spoofing attacks are more challenging to detect than ground-based spoofing attacks, motivating our research and contribution. Figure 9 also

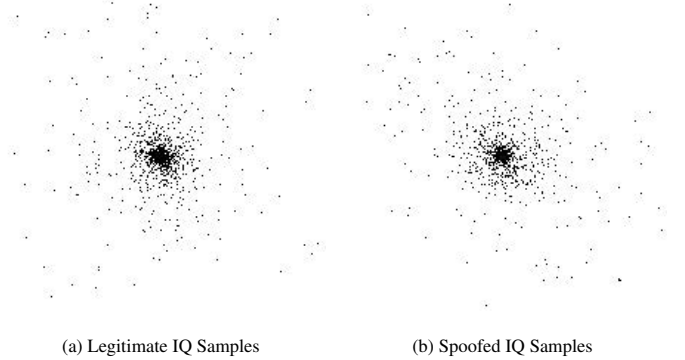


Figure 7: $N = 1,000$ I-Q samples as received from legitimate satellites (a) and drones (b).

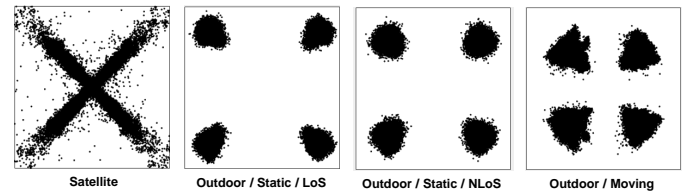


Figure 8: IQ samples collected as part of the analysis in [11], received on an Ettus X310 from (i) Satellite, (ii) Spoofer deployed Outdoors, with Static LoS, (iii) Spoofer deployed Outdoors, with Static NLoS, and (iv) Spoofer deployed Outdoors and moving. Each sub-figure reports a subset of 10,000 I-Q samples randomly taken from the collected measurements.

reports the distribution of the SNR of legitimate and spoofed messages when $N = 1,000$ and $N = 250$. We computed the

SNR according to the geometrical formula given in Eq. 8 [49].

$$\begin{aligned}
 SNR &= P(r) - P(n) \\
 &= 10 \cdot \log_{10}(I^2 + Q^2) - 10 \cdot \log_{10}((I-1)^2 + Q^2) \\
 &= 10 \cdot \log_{10} \frac{I^2 + Q^2}{(I-1)^2 + Q^2}.
 \end{aligned} \tag{8}$$

We notice minimal differences in the SNR values of legitimate

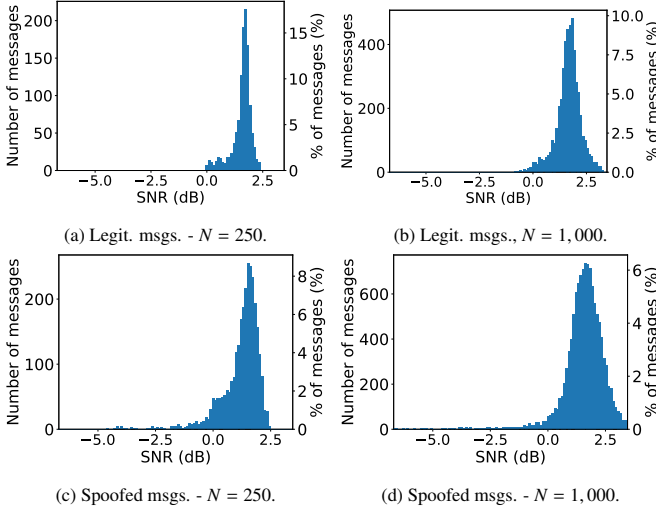


Figure 9: Distribution of the SNR of received legitimate (a, b) and spoofed (c, d) IRIDIUM messages.

and spoofed signals. Taking into account the images generated from $N = 250$ samples, only 7.7% of the images generated from the spoofed samples report SNR values outside of the interval of SNR values characterizing images generated from legitimate samples, which is $[0, 2.5]$ dBm. Similarly, when considering images generated from $M = 1,000$ samples, the overlap area between the two distributions reduces further to 3.3%. These results indicate that, independently of the number of samples, we cannot classify the images (or the associated IQ samples) as legitimate or spoofed by only looking at the SNR, suggesting the need for a tailored detection solution.

7. Experimental Performance Analysis

In this section, we report the main results of our experimental performance assessment. We explain the metrics used for our results in Sec. 7.1 and report our results in Sec. 7.2.

7.1. Metrics

In the following, we report the performance of all the tested solutions using the Area Under-the-Curve (AUC) of the Receiver Operating Characteristic (ROC) curve. The ROC curve plots the True Positive Rate (TPR) against the False Positive Rate (FPR) at various threshold settings. Therefore, the ROC curve inherently depends on how false positives (FP) vary with different classification thresholds. The AUC is the area under this

ROC curve, so it summarizes how well the classifier distinguishes between classes across all thresholds, taking into account both true positives and false positives [50]. This metric ranges between the values 0 and 1, with 0.5 representing a random guess and 1 indicating a perfect classification. Note that the ROC AUC measures the quality of a classifier independently of the threshold selection process, and it is recommended when the datasets are unbalanced, as it evaluates the trade-off between sensitivity (true positive rate) and specificity (true negative rate) in various threshold settings [51], [52].

For each reported figure, we train our proposed solution as outlined in Sec. 5, using 80% of the images generated from legitimate samples. We validate the model using the remaining 20% and then test it using spoofed data acquired in a particular scenario, as described in Sec. 6. We use K-fold validation with $K = 5$ for each configuration and report the quantiles 0.05, 0.5, and 0.95 for the ROC AUC values. Finally, we compare our proposed solution against two benchmarks, i.e., the solution in [11], using a binary Fully Convolutional Data Descriptor (FCDD) to detect spoofing attacks [53], and the proposal in [9], using the neural network *Resnet-18* to authenticate satellite wireless messages. Note that the proposal in [11] considers the same problem tackled in this manuscript. Thus, no changes are needed to ensure a fair comparison. Conversely, to allow for a fair comparison between our setup and the proposal in [9], we use the neural network classifier *Resnet-18* to distinguish between satellite (authorized) and drone (unauthorized) transmissions using binary classification.

We ran all data analyses on the High-Performance Computing (HPC) cluster provided by TU/e, Eindhoven, Netherlands, including a CPU AMD EPYC 7313 running at 3.00 GHz, 16 GB of RAM, and a TESLA V100 GPU with 16GB of RAM.

7.2. Results

We report in Fig. 10 (a-c) the performance of our solution in the three investigated scenarios, using various numbers of samples per image N (recall Sec. 5.1). In the vast majority of cases, the protocol configuration using $N = 1,000$ samples per image outperforms the configurations using fewer samples, demonstrating that, generally speaking, using a higher number of samples per image increases spoofing detection robustness. This finding is likely due to the fact that using more samples per image helps to better isolate outlier samples. When histograms are not used for generating images, such outliers have the same relative weight in the image as the other samples, thus negatively influencing the detection process. We notice just a few cases where using fewer samples per image achieves higher values of the ROC AUC, e.g., S1 at 90 m and S2 at 70 m. In these few cases, we notice more noise affecting the collected data; thus, using limited samples per image with noisy data can improve the performance by reducing the impact of the noise. Overall, with $N = 1,000$ samples per image, our solution can detect spoofing attacks with remarkable accuracy, i.e., with an average ROC AUC always higher than 0.8 in S1, 0.75 in S2 and 0.99 in S3. Considering that IRIDIUM satellites transmit at 50 kbps, we need 20 ms to acquire such a number of samples, while running the AE requires only a few ms. In all scenarios,

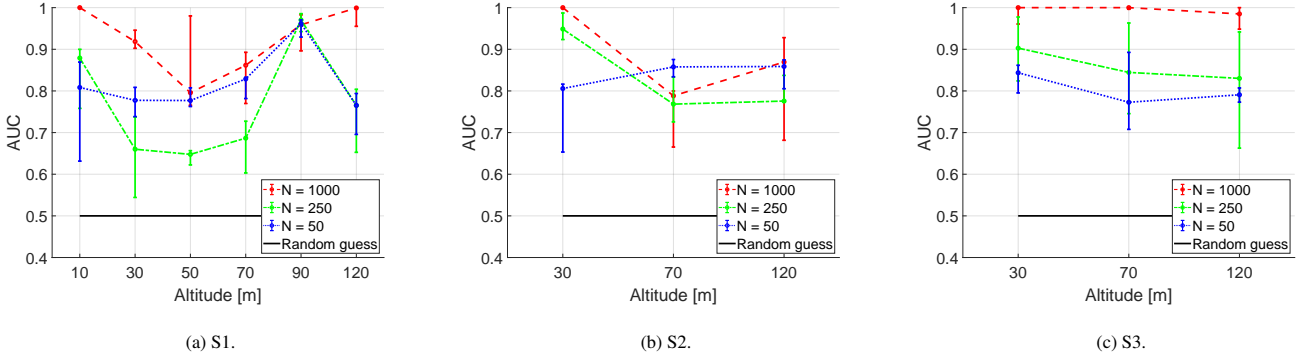


Figure 10: Performance of our solution in S1 (a), S2 (b), and S3 (c), with $N = 50$, $N = 250$, and $N = 1,000$ samples per image.

we also see a general decreasing trend in the performance of our solution with the increase of the altitude of the spoofing drone. Such results confirm that, to increase the chances of bypassing our solution, the spoofing drone should exceed the maximum height imposed by law regulations and get as high as possible in the sky, closer to the satellites, to imitate the (satellite) fading characteristics more effectively. Besides being against the law, such requirement also forces the attacker to use more powerful and expensive drones, capable of flying at very high altitudes. We also highlight that, as shown by the results in Fig. 10(c), the receiver movement introduced in S3 improves performance compared to other scenarios, with any value of N . This result is particularly promising for the application of our solution on mobile entities, e.g., vehicles or drones, which already move as part of their regular operations.

We also measured the overhead of our solution, i.e., the time required to generate an image from incoming IQ samples, namely τ_{img} , and the time to classify such image as benign or spoofed, namely τ_{ae} . We also estimated the memory requirements of our solution, i.e., the size on disk of the model (M_{ae}) and the size of the image on disk with various no. of samples M_{image} . We report the results in Tab. 4. We notice that collecting sam-

Samples per Image (N)	250	500	1000
τ_{img} (ms)	0.0085	0.0089	0.0102
τ_{ae} (ms)	0.0027	0.0028	0.0032
M_{ae} (MB)	13	13	13
M_{image} (KB)	3.6	4.35	5.76

Table 4: Overhead components of our solution.

ples necessary to generate an image with $N = 250$, $N = 500$, or $N = 1,000$ samples is in the order of a few micro-seconds ($10 \mu\text{sec}$ with $N = 1,000$ samples). Even in the worst case where we use $N = 1,000$, the time to classify such an image as benign or malicious on our computing equipment is very limited, i.e., 0.032 msec, and the generated model requires only 13 MB of storage space. Therefore, the computational cost of the solution is very limited, as well as its storage requirements are limited for regular computing units. We further consider the configuration of our solution using $N = 250$ samples per image (often performing the worst in Fig. 10), and we also compare the performance of our proposed solution to the

benchmarks proposed by Oligeri et al. in [11] and [9]. We report the results of our comparison in Figs. 11(a-c). We observe that our proposed approach consistently outperforms the benchmark solutions in all conditions. In fact, in all the investigated scenarios and altitudes, the two benchmarks rarely exceed a ROC AUC value of 0.6, indicating that they can hardly detect spoofing activity. The solution using *Resnet-18* proposed in [9] is the least effective, being characterized by an average accuracy equivalent to random guess, i.e., $ROCAUC = 0.5$. This is due to the reduced number of samples used to build the corresponding images. Indeed, as highlighted by the authors in [9], PAST-AI requires approximately 10^6 samples to perform reliably, which is not feasible when performing spoofing attack detection. The solution using the FCDD network proposed in [18] is usually slightly more effective than the previous one but less effective than our proposed approach. We notice only one experiment where the solution in [11] achieves slightly higher performance, i.e., S1 with the drone spoofing at 90 m. Comparing Fig. 11(a) with Fig. 10(a), we can see that the performance of the benchmark aligns with the one achieved by our solution using $N = 1,000$ samples per image; we believe that this result is due to the binary nature of the FCDD used in [11], which could potentially better discriminate spoofed from legitimate samples, since it is exposed to both classes during training. However, as mentioned earlier, collecting attack samples for the training process is often infeasible due to the required technical skills, expensive equipment, and law regulations. Our solution, using fewer samples per image, can provide similar results while requiring only regular satellite data (no anomalous samples at testing time). This feature further emphasizes the practical value of the proposed approach. Moreover, note that (aerial) spoofing can occur via various scenarios and channel conditions, being quite hard to model precisely through a binary classifier. Our proposed approach, requiring modeling only the regular profile of the received messages, is often even more successful than binary classification approaches in detecting anomalies.

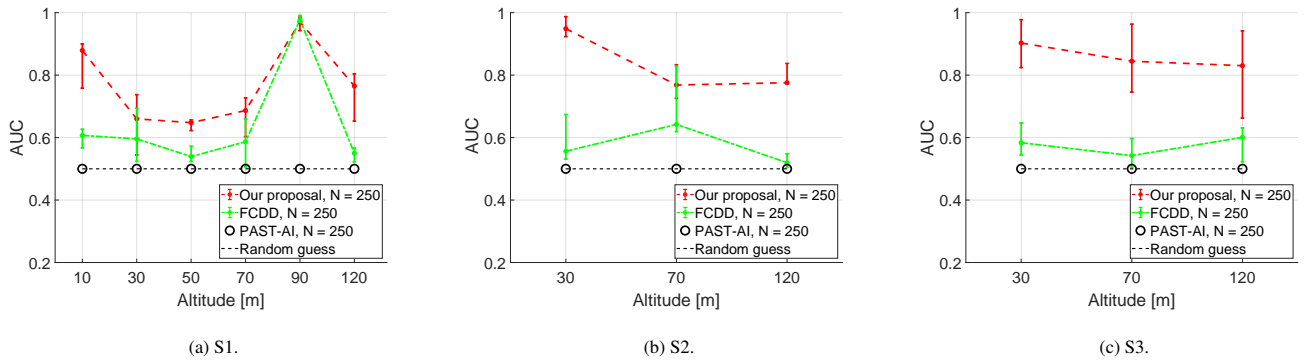


Figure 11: Performance of our solution and the benchmarks in [11] and [9] in scenarios S1 (a), S2 (b), and S3 (C), using $N = 250$ samples per image.

8. Discussion

Implications for Practice. The results provided in Sec. 7.2 indicate that, through our solution, we can detect spoofing attacks to LEO satellite communication systems originating by drones by analyzing the physical-layer signals at the satellite receiver, and looking for anomalies in the received signal. At the same time, especially when considering $N = 50$ samples per image, the average optimal ROC AUC values sometimes do not exceed the value 0.75. While such performances are considerably higher than the state of the art (see Fig. 11), they are not high enough to provide reliable detection in real-world systems. Thus, we foresee that our solution could be used to provide an additional layer of security to existing security systems, rather than as a standalone solution. This is common to many security systems analyzing wireless signals, e.g., Radio Frequency Fingerprinting [9]. We also notice that detection accuracy improves when there are more samples available per message and when the receiver is mobile (see Fig. 11 (c)). Thus, whenever possible, receivers should oversample the incoming signal and move periodically to maximize detection accuracy and reduce false positives.

Limitations. The results reported in Fig. 10 and Fig. 11 suggest that the attacker can increase the chances of bypassing our solution by flying higher, so better mimicking the satellite communication channel. However, due to the regulations in place in our region, in this research, we conducted tests with a drone flying at the maximum altitude of 120 m—being the maximum allowed altitude [48]. We acknowledge that attackers could neglect such regulations and execute advanced spoofing strategies by flying the drone at a higher altitude. Future research could test our solution with data collected in regions with more relaxed regulations, investigating further the capabilities of advanced attackers. Our tests were also executed in large rural areas, so to minimize safety concerns. Future research could test our solution with data collected in urban environments, to check if reflections caused by man-made constructions could help the attacker, or strengthen the defense strategy.

9. Conclusion and Future Work

In this paper, we proposed a new solution for detecting aerial spoofing attacks to LEO satellite communication systems, using a sparse Autoencoder. Our proposed solution requires converting received Physical information (IQ samples) into images and then using an Autoencoder to identify which of them come from the spoofer. We validated our solution using data collected through an extensive real-world measurement campaign, encompassing actual spoofing attacks of a reference LEO satellite system (IRIDIUM) via a Software-Defined Radio installed on a drone and flown in a remote area via several attack scenarios (static, transmitter movement, transmitter and receiver movement). Our proposed solution can detect aerial spoofing attacks with a minimum ROC AUC value of 0.75, systematically outperforming competing approaches. We also released the dataset collected for this study as open source to the research community, contributing to stimulating further real-world applied research on satellite security. Note that, in our work, we could not fly the drone beyond the maximum altitude of 120 m imposed by EU regulations. Also, we did not carry out tests in an urban scenario, where the presence of man-made construction and people's movement might change the profile of the signal received from satellites. In line with such limitations, in future work, we plan to test our solution in urban environments, so to assess the impact of man-made constructions on the effectiveness of our approach. Moreover, we will work on an analytical channel model for LEO satellite transmissions to analyze the performance of our solution in the presence of attackers circumventing law regulations on the maximum allowed flight altitude of drones. Finally, we will investigate the feasibility of detecting advanced drone-based LEO spoofing attacks onboard other drones and LEO satellites.

References

- [1] F. Prol, R. Ferre, Z. Saleem, et al., "Position, navigation, and timing (PNT) through low earth orbit (LEO) satellites: A survey on current status, challenges, and opportunities," *IEEE Access*, vol. 10, pp. 83 971–84 002, 2022.
- [2] L. Zhao, S. Geng, X. Tang, A. Hawbani, Y. Sun, L. Xu, and D. Tarchi, "ALANINE: A Novel Decentralized Personalized Federated Learning For

- Heterogeneous LEO Satellite Constellation,” *IEEE Transactions on Mobile Computing*, pp. 1–16, 2025.
- [3] L. Zhao, Y. Liu, A. Hawbani, N. Lin, W. Zhao, and K. Yu, “QoS-Aware Multihop Task Offloading in Satellite–Terrestrial Edge Networks,” *IEEE Internet of Things Journal*, vol. 11, no. 19, pp. 31 453–31 466, 2024.
 - [4] J. Merwe, X. Zubizarreta, I. Lukćin, et al., “Classification of Spoofing Attack Types,” in *European Navigation Conf.*, 2018, pp. 91–99.
 - [5] E. Salkield, M. Szakály, J. Smailes, et al., “Satellite spoofing from a to z: on the requirements of satellite downlink overshadowing attacks,” in *Proc. of ACM Conf. on Security and Privacy in Wireless and Mobile Networks*, 2023, pp. 341–352.
 - [6] B. Cyr, Y. Long, T. Sugawara, and K. Fu, “Position Paper: Space System Threat Models Must Account for Satellite Sensor Spoofing,” in *SpaceSec*, 2023.
 - [7] P. Yue, J. An, J. Zhang, et al., “Low Earth Orbit Satellite Security and Reliability: Issues, Solutions, and the Road Ahead,” *IEEE Communications Surveys & Tutorials*, 2023.
 - [8] P. Tedeschi, S. Sciancalepore, and R. Di Pietro, “Satellite-based communications security: A survey of threats, solutions, and research challenges,” *Computer Networks*, vol. 216, p. 109246, 2022.
 - [9] G. Oliveri, S. Sciancalepore, S. Raponi, et al., “PAST-AI: Physical-layer authentication of satellite transmitters via deep learning,” *IEEE Trans. on Information Forensics and Security*, vol. 18, pp. 274–289, 2023.
 - [10] A. Sadighian, S. Sciancalepore, and G. Oliveri, “FadePrint: Satellite spoofing detection via fading fingerprinting,” in *2024 IEEE 21th Consumer Communications & Networking Conf. (CCNC)*, 2024.
 - [11] G. Oliveri, S. Sciancalepore, and A. Sadighian, “SatPrint: Satellite link fingerprinting,” in *2024 ACM Symposium on Applied Computing (SAC)*, 2024, pp. 177–185.
 - [12] R. Kumar and S. Arnon, “Leveraging Atmospheric Effects with LSTM for Ensuring Cybersecurity of Satellite Links,” *Authorea Preprints*, 2023.
 - [13] J. Wigchert, “Aerial Spoofing Detection Dataset,” 2023, accessed: 2025-May-08. [Online]. Available: <https://github.com/JosWigchert/AerialSpoofingDetectionDataset>
 - [14] T. S. Rappaport, *Wireless Communications: Principles and Practice*. Cambridge University Press, 2024.
 - [15] A. Al-Shawabka, F. Restuccia, S. D’Oro, et al., “Exposing the Fingerprint: Dissecting the Impact of the Wireless Channel on Radio Fingerprinting,” in *IEEE Conf. on Computer Communications*, 2020, pp. 646–655.
 - [16] Iridium Inc., “Network — Iridium Satellite Communications,” <https://www.iridium.com/network/>, accessed: 2025-May-08. [Online]. Available: <https://www.iridium.com/network/>
 - [17] —, “Iridium Communications Inc. 2023 Fact Sheet,” 2024, accessed: 2025-May-08. [Online]. Available: https://filecache.investorroom.com/mr5ir-iridium/741/2023_Fact_Sheet_Iridium_Communications.pdf
 - [18] G. Oliveri, S. Sciancalepore, and R. Di Pietro, “GNSS spoofing detection via opportunistic IRIDIUM signals,” in *Proc. of the 13th ACM Conf. on Security and Privacy in Wireless and Mobile Networks*, 2020, pp. 42–52.
 - [19] S. Pratt, R. Raines, C. Fossa, et al., “An operational and performance overview of the IRIDIUM low earth orbit satellite system,” *IEEE Communications Surveys*, vol. 2, no. 2, pp. 2–10, 1999.
 - [20] muccc, “gr-iridium,” <https://github.com/muccc/gr-iridium>, 2024, accessed: 2025-May-08.
 - [21] D. Mackay, “Iridium Makes Strategic Investment in DDK Positioning, Provider of Enhanced GNSS Accuracy Solutions,” *DDK Positioning News*, May 2021, accessed: 2025-May-08. [Online]. Available: <https://www.ddkpositioning.com/iridium/>
 - [22] Iridium Inc., “What is Satellite IoT and How is it Used?” <https://www.iridium.com/blog/what-is-satellite-iot-and-how-is-it-used/>, accessed: 2025-May-08. [Online]. Available: <https://www.iridium.com/blog/what-is-satellite-iot-and-how-is-it-used/>
 - [23] P. Li, Y. Pei, and J. Li, “A comprehensive survey on design and application of autoencoder in deep learning,” *Applied Soft Computing*, vol. 138, p. 110176, 2023.
 - [24] S. Sciancalepore, F. Kusters, N. K. Abdelhadi, and G. Oliveri, “Jamming Detection in Low-BER Mobile Indoor Scenarios via Deep Learning,” *IEEE Internet of Things J.*, vol. 11, no. 8, pp. 14 682–14 697, 2024.
 - [25] J. Zhou, X. Li, T. Ding, C. You, Q. Qu, and Z. Zhu, “On the Optimization Landscape of Neural Collapse under MSE Loss: Global Optimality with Unconstrained Features,” in *Proc. of the 39th International Conf. on Machine Learning*, vol. 162, Jul 2022, pp. 27 179–27 202.
 - [26] V. Škvára, J. Francá, M. Zorek, T. Pevný, and V. Šmídl, “Comparison of Anomaly Detectors: Context Matters,” *IEEE Transactions on Neural Networks and Learning Systems*, vol. 33, no. 6, pp. 2494–2507, 2021.
 - [27] X. Wang, L. Gao, S. Mao, and S. Pandey, “DeepFi: Deep learning for indoor fingerprinting using channel state information,” in *IEEE Wireless Communications and Networking Conf.*, 2015, pp. 1666–1671.
 - [28] M. Foruhandeh, A. Mohammed, G. Kildow, et al., “Spotr: GPS Spoofing Detection via Device Fingerprinting,” in *Proc. of ACM Conf. on Security and Privacy in Wireless and Mobile Networks*, 2020, p. 242–253.
 - [29] C. Sun, J. Cheong, A. Dempster, et al., “Robust Spoofing Detection for GNSS Instrumentation Using Q-Channel Signal Quality Monitoring Metric,” *IEEE Trans. on Instrumentation and Measurement*, vol. 70, pp. 1–15, 2021.
 - [30] Y. Chapre, A. Ignjatovic, A. Seneviratne, and S. Jha, “CSI-MIMO: An efficient Wi-Fi fingerprinting using Channel State Information with MIMO,” *Pervasive and Mobile Computing*, vol. 23, pp. 89–103, 2015.
 - [31] M. Psiaki, B. O’Hanlon, W. Brady, et al., “GPS Spoofing Detection via Dual-Receiver Correlation of Military Signals,” *IEEE Trans. on Aerospace and Electronic Systems*, vol. 49, no. 4, pp. 2250–2267, 2013.
 - [32] J. Hua, H. Sun, Z. Shen, et al., “Accurate and Efficient Wireless Device Fingerprinting Using Channel State Information,” in *IEEE Conf. on Computer Communications*, 2018, pp. 1700–1708.
 - [33] A. Broumandan, J. Jafarnia-Jahromi, V. Dehghanian, et al., “GNSS spoofing detection in handheld receivers based on signal spatial correlation,” in *Proc. of IEEE/ION Position, Location and Navigation Symp.*, 2012, pp. 479–487.
 - [34] M. Abdrabou and T. A. Gulliver, “Physical Layer Authentication for Satellite Communication Systems Using Machine Learning,” *IEEE Open Journal of the Communications Society*, vol. 3, pp. 2380–2389, 2022.
 - [35] —, “Game Theoretic Spoofing Detection for Space Information Networks Using Physical Attributes,” *IEEE Transactions on Communications*, 2024.
 - [36] D. Schmidt, K. Radke, S. Camtepe, et al., “A Survey and Analysis of the GNSS Spoofing Threat and Countermeasures,” *ACM Comput. Surv.*, vol. 48, no. 4, may 2016.
 - [37] D. He, S. Chan, and M. Guizani, “Communication Security of Unmanned Aerial Vehicles,” *IEEE Wireless Communications*, vol. 24, no. 4, pp. 134–139, 2016.
 - [38] G. Oliveri, S. Sciancalepore, O. A. Ibrahim, and R. Di Pietro, “Gps spoofing detection via crowd-sourced information for connected vehicles,” *Computer Networks*, vol. 216, p. 109230, 2022.
 - [39] S. Alhazbi, S. Sciancalepore, and G. Oliveri, “The Day-After-Tomorrow: On the performance of radio fingerprinting over time,” in *Proc. of the 39th Annual Computer Security Applications Conf.*, 2023, pp. 439–450.
 - [40] J. Smailes, S. Köhler, S. Birnbach, M. Strohmeier, and I. Martinovic, “Watch This Space: Securing Satellite Communication through Resilient Transmitter Fingerprinting,” in *Proceedings of the 2023 ACM SIGSAC Conference on Computer and Communications Security*, 2023, pp. 608–621.
 - [41] C. Solenthaler and J. S. M. Strohmeier, “OrbID: Identifying Orbcomm Satellite RF Fingerprints,” *3rd Workshop on the Security of Space and Satellite Systems*, 2025.
 - [42] P. Borhani-Darian, H. Li, P. Wu, and P. Closas, “Detecting GNSS spoofing using deep learning,” *EURASIP Journal on Advances in Signal Processing*, vol. 2024, no. 1, p. 14, 2024.
 - [43] I. Goodfellow, Y. Bengio, A. Courville, and Y. Bengio, *Deep Learning*. MIT press Cambridge, 2016, vol. 1, no. 2.
 - [44] S. Erfani, S. Rajasegarar, S. Karunasekera, et al., “High-dimensional and large-scale anomaly detection using a linear one-class SVM with deep learning,” *Pattern Recognition*, vol. 58, pp. 121–134, Oct. 2016.
 - [45] Nooelec, “Nooelec SAWbird+ IR - Premium SAW Filter & Cascaded Ultra-Low Noise LNA Module for Iridium and Inmarsat Applications. 1620MHz Center Frequency,” <https://www.nooelec.com/store/sdr/sdr-addons/sawbird/sawbird-plus-ir-304.html>.
 - [46] J. Young, “How much weight can a drone carry? real cases (lbs & kg),” Jul 2023. [Online]. Available: <https://www.droneguru.net/weight-a-drone-carry/>
 - [47] Droneblog, “Drone Payload: What Can a Drone Carry?” <https://www.droneblog.com/drone-payload/>, 2024, accessed: 2025-May-08.

- [48] Human Environment and Transport Inspectorate, "Drones for residents of the European Union," <https://english.ilent.nl/topics/rpas---remotely-piloted-aircraft-systems-drones>, 2024.
- [49] M. Irfan, S. Sciancalepore, and G. Oligeri, "Preventing Radio Fingerprinting through Friendly Jamming," 2024. [Online]. Available: <https://arxiv.org/abs/2407.08311>
- [50] C. M. Bishop, *Pattern recognition and machine learning* by Christopher M. Bishop. Springer Science+ Business Media, LLC, 2006.
- [51] S. S. Khan and B. Taati, "Detecting unseen falls from wearable devices using channel-wise ensemble of autoencoders," *Expert Systems with Applications*, vol. 87, pp. 280–290, 2017.
- [52] F. Angiulli, F. Fassetti, and L. Ferragina, "Reconstruction Error-based Anomaly Detection with Few Outlying Examples," 2024. [Online]. Available: <https://arxiv.org/abs/2305.10464>
- [53] Liznerski, P. et al., "Explainable Deep One-Class Classification," in *Int. Conf. on Learn. Representat.*, 2021.